ELSEVIER

Journal of Power Sources 87 (2000) 92–100

JOURNAL OF POWER SOURCES

www.elsevier.com/locate/jpowsour

Microstructure and cathodic performance of $La_{0.9}Sr_{0.1}MnO_3$ electrodes according to particle size of starting powder

Jin H. Choi, Jong H. Jang, Ji H. Ryu, Seung M. Oh *

Division of Chemical Engineering and Institute of Chemical Process, College of Engineering, Seoul National University, Seoul 151-742, South Korea

Received 10 August 1999; accepted 2 September 1999

Abstract

Three $La_{0.9}Sr_{0.1}MnO_3$ (LSM)/YSZ (yttria-stabilized zirconia) electrodes are prepared from LSM powders of different particle size via the silk-printing technique. The mean particle size of the three LSM powders is 1.54, 5.98 and 11.31 μm, respectively. The microstructural changes evolved during the course of electrode adhesion and half-cell operation are traced by taking scanning electron micrographs, and the cathodic activity is measured at 900°C in air using AC impedance spectroscopy. The LSM1 electrode prepared from the smallest powder shows good initial activity, but a rapid decrease in activity along with notable particle growth is observed within a short period of time. By contrast, the LSM3 electrode fabricated with the largest powder has a poor initial activity but the loss in activity is not appreciable as particle growth is insignificant. The LSM2 electrode that is prepared from medium-sized powder gives the best performances in terms of initial activity and long-term stability. It is likely that the LSM2 electrode has a larger number of active sites for the oxygen reduction reaction than LSM3 and the loss of active sites due to particle growth is less severe than with the LSM1 electrode.

Keywords: Solid oxide fuel cells; Strontium-doped lanthanum manganites ($La_{0.9}Sr_{0.1}MnO_3$); AC impedance spectroscopy; Electrochemical O_2 reduction

1. Introduction

At present, strontium-doped lanthanum manganites ($La_{1-x}Sr_xMnO_3$ = LSM) are widely studied for their application as cathode materials in solid oxide fuel cells (SOFCs). This material has a high electrical conductivity in an oxidizing atmosphere and good high-temperature phase stability. Also, its thermal expansion coefficient is close to that of yttria-stabilized zirconia (YSZ) electrolyte [1].

It has been generally accepted that the electrochemical reduction of oxygen on SOFC cathodes takes place at either the three-phase boundary (TPB) sites or the electrode surface sites as determined by the oxide conductivity of the electrode materials [2–9]. The former are the contacting points developed at the electrode particles/YSZ electrolyte interface, whereas the latter are the whole electrode surface sites developed in the porous electrode layer. It is proposed that the O_2 reduction reaction on highly O^{2-} conducting materials (for example, cobalt perovskites) can take place at the electrode surface sites as well as the TPB sites since bulk diffusion of O^{2-} is possible with a high oxide vacancy concentration [2,3]. By contrast, the active sites in the electrode materials which have a lower O^{2-} conductivity, due to a low oxide vacancy concentration (for example, LSM), are considered to be largely limited to the TPB sites [4–6]. With an expectation, however, that the surface or grain boundary diffusion of O^{2-} ions in porous electrodes is appreciable with a much faster rate than the bulk diffusion, several studies [7–9] have proposed that the LSM electrode surface sites exposed near the YSZ surface can also participate in the cathodic reaction.

The microstructure of the electrode layer is the critical factor in determining the cathodic activity, regardless of the nature of the active sites involved. For high activity, the cathode layer should have rich LSM grains/YSZ-surface contact points (TPB sites) or the LSM particle surface should be highly exposed near the YSZ surface region (electrode surface sites). Also, a high porosity is desirable to allow gas-phase oxygen to reach both sites.

In general, the electrode microstructure is controlled by several preparation variables, i.e., the particle size of elec-

* Corresponding author. Tel.: +82-2-880-7074; fax: +82-2-888-1604; e-mail: seungoh@plaza.snu.ac.kr

0378-7753/00/$ - see front matter
PII: S0378-7753(99)00365-1

trode materials, heating condition for electrode adhesion, and cell operation conditions. Concerning the particle size of electrode materials, a higher activity is expected with smaller particles because a larger number of TPB or electrode surface sites along with a higher porosity can be developed. Because the smaller particles are, however, more vulnerable to sintering under the high temperature electrode adhesion and cell operation conditions, the use of smaller powders can not always guarantee a higher activity. Particle growth leads to a loss of active sites. A trade-off is thus expected at a certain range of particle size between the two conflicting factors, namely, the number of active sites and particle sintering.

In this study, the microstructure of LSM electrodes was controlled by varying the particle size of the starting powders while keeping the other variables fixed. Three LSM/YSZ electrodes were fabricated using three LSM powders of different sizes. The microstructural change was traced by taking scanning electron micrographs at each preparation step. The cathodic activity was monitored by estimating the charge transfer resistance values with half-cell operations, and the results were correlated to the microstructural change.

2. Experimental

2.1. Powder synthesis and characterization

The $La_{0.9}Sr_{0.1}MnO_3$ powders of different particle size were prepared by varying the synthetic method and calcination temperature [10]. For the LSM1 powder, the precursor was prepared by the Pechini method and calcined at 800°C in air. The precursors of LSM2 and LSM3 were synthesized by the citrate method, and were calcined at 800 and 1000°C, respectively. The synthetic scheme is provided in Fig. 1, where the left panel corresponds to the citrate method and the right one to the Pechini method. For the citrate synthesis, the nitrate salts of La, Sr, and Mn were dissolved in water with a molar ratio of 9:1:10, and then citric acid (Aldrich, 99.5 + %) equal to 1.2 times the total metal content was added. The precursor gel was made after drying the solution at 70°C in a vacuum oven, then the gel was crushed, charred at 300°C in air, and calcined. For the Pechini synthesis, an equimolar amount of ethylene glycol (Aldrich, 99.5 + %) to citric acid was added to the metal ion solutions. After polymerizing at 130°C for 30 min, the residue was charred at 300°C and calcined at

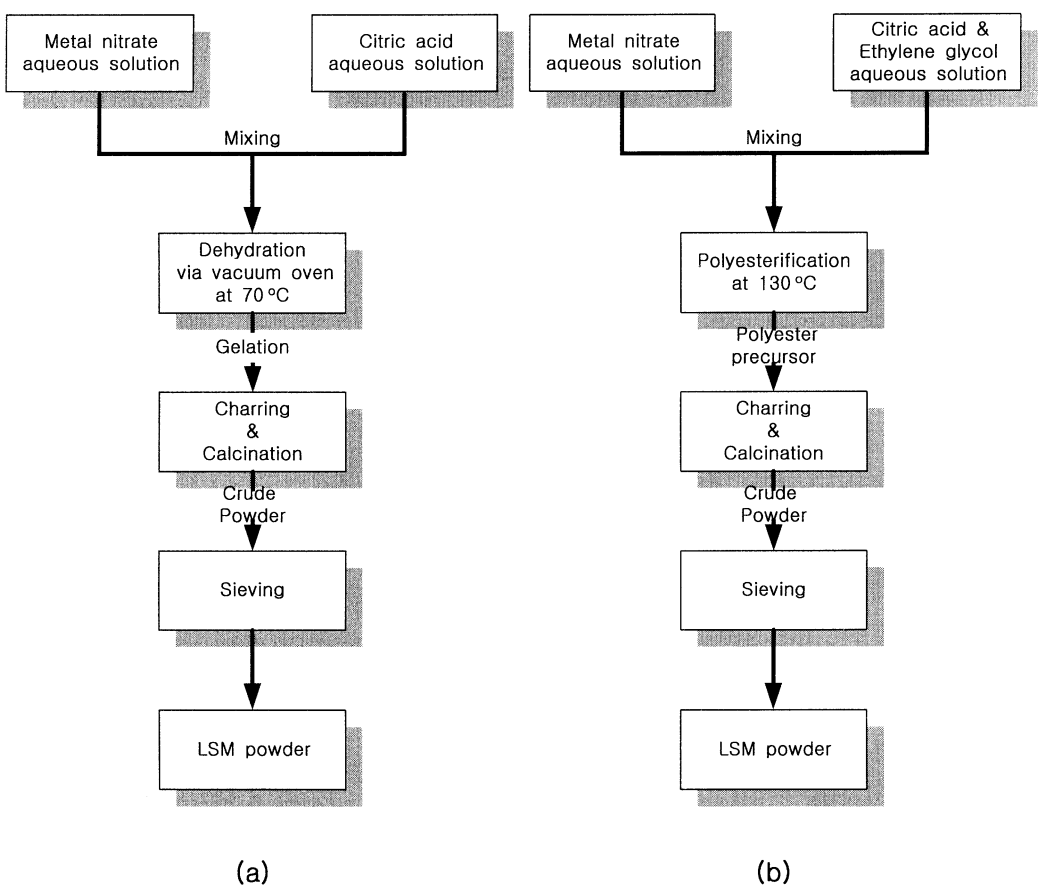

Fig. 1. Synthetic procedures for (a) citrate and (b) Pechini methods.

800°C. For both syntheses, the heating and cooling rate was controlled at 2°C min^{-1} and the calcination was performed for 6 h. The final powders were obtained after crushing and passing through a standard 400 mesh sieve. X-ray diffraction (XRD) analysis was performed by means of a Rigaku diffractometer using Cu Kα (= 1.5418 Å) as the target. To analyze the particle size distribution, the powder was ultrasonically dispersed in water for 24 h to prevent agglomerations. The Malvern Mastersizer was used for this purpose.

2.2. Fabrication of half-cells and electrochemical characterization

The cathodic performance was analyzed with a three-electrode configuration. For electrode fabrication, the LSM powder was dispersed in turpentine oil and silk-printed on the surface of an 8 mol% YSZ disk (diameter = 1.8 cm, thickness = 0.1 cm) by using a 100 mesh silk screen. Electrode adhesion was carried out at 1200°C for 2 h in air. For reference and counter electrodes, Pt paste (Ferro, #4082) was deposited on the other side of the YSZ disk, using a 100-mesh silk screen, and then heat-treated at 1000°C for 2 h. The areas of the working, counter and reference electrode were 0.22, 1.17 and 0.15 cm^2, respectively. For electrical contact, a piece of Pt gauze was placed on the electrode surfaces and pressure-contacted by a spring.

The half-cell characteristics of the LSM/YSZ electrodes were analyzed at 900°C by using AC impedance spectroscopy. Air was passed through both the cathodic and anodic sides of the cells. The impedance analysis was conducted by means of an EG&G PARC 173 potentiostat, 276 interface and a 5208 lock-in analyzer. The frequency range was 0.05 Hz–100 kHz and the AC amplitude was

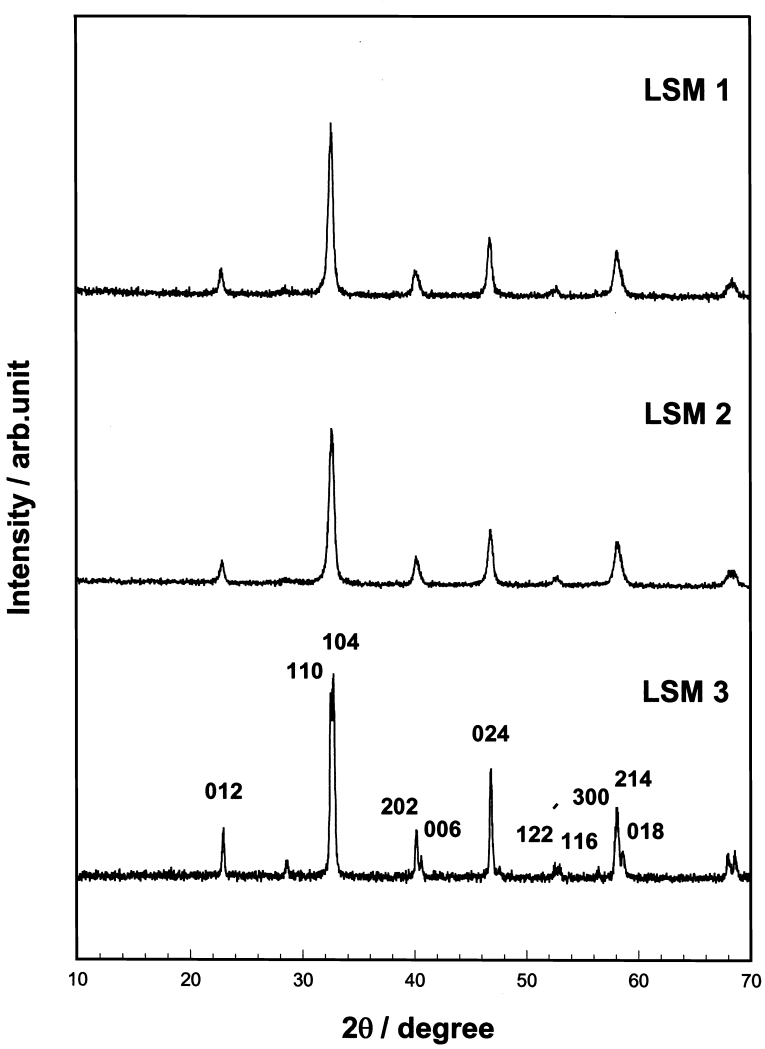

Fig. 2. X-ray diffraction patterns observed with $La_{0.9}Sr_{0.1}MnO_3$ powders. Peak indexing with a rhombohedral lattice ($a = b = c = 5.53$ Å, $\alpha = \beta = \gamma = 60.5°$) is indicated in LSM3.

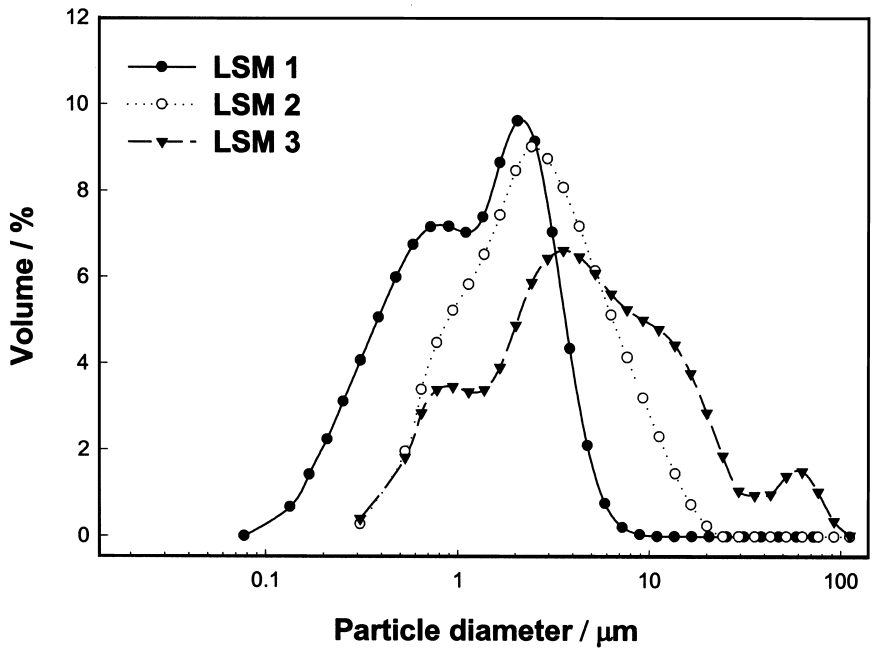

Fig. 3. Particle-size distributions of synthesized $La_{0.9}Sr_{0.1}MnO_3$ powders.

fixed at 10 mV. For data analysis, non-linear least-squares fitting was performed using the EQUIVCRT program [11].

Steady-state polarization measurements were made with an EG&G PARC 173 potentiostat and a 276 interface at a scan rate of 0.05 mV s^{-1} from 0 to 1000 mV. The *iR*-drop due to the electrolyte resistance was corrected by subtracting the R_1 values that were obtained from the AC impedance measurements.

The microstructural change of the LSM electrodes was monitored using a scanning electron microscope (SEM, JEOL 840A). Three micrographs for each electrode were taken after silk printing, electrode adhesion and 100 h of cell operation, respectively.

3. Results and discussion

3.1. Powder characteristics of $La_{0.9}Sr_{0.1}MnO_3$

The XRD patterns of the synthesized LSM powders are shown in Fig. 2, where it is seen that the synthesized perovskite materials have a rhombohedral structure without discernible impurity phases. The diffraction lines ob-

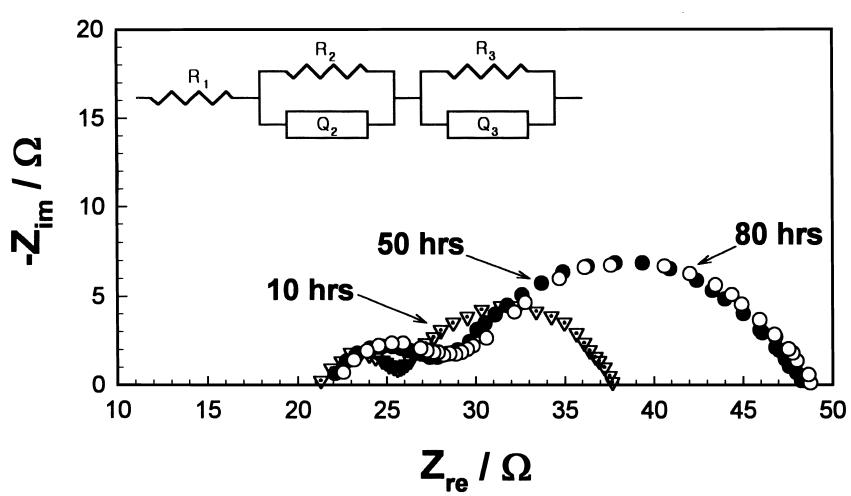

Fig. 4. Evolution of AC impedance spectra recorded with LSM1 electrode at 900°C in air as a function of operation time. Note that the spectra are composed of two depressed semi-circles. The best-fitted equivalent circuit is depicted in the inset.

Table 1
AC impedance parameters obtained LSM1 electrode after deconvoluting observed spectra
Q is the circuit description code (CDC) which represents the constant phase element (CPE). Representation of CPE in admittance is $Y(\omega) = Y_0(j\omega)^n$.

Time (h)	R_1 (Ω)	R_2 (Ω)	Q_2		R_3 (Ω)	Q_3	
			Y_0	n		Y_0	n
5.3	21.4	3.1	3.0E-6	1.00	8.0	9.5E-4	0.83
21.1	21.8	4.4	6.0E-6	0.93	15.5	1.2E-3	0.76
36.8	21.9	5.3	1.2E-5	0.86	18.3	1.2E-3	0.75
52.8	22.1	5.8	1.4E-5	0.83	20.3	1.3E-3	0.73
68.9	22.3	5.9	1.2E-5	0.84	20.3	1.2E-3	0.73
84.8	22.5	6.2	1.2E-5	0.84	20.2	1.2E-3	0.74
116.4	22.7	6.3	9.8E-6	0.86	20.3	1.2E-3	0.72

served with LSM3 were indexed with the rhombohedral lattice [12,13], but the indexing was impossible with the other profiles due to line broadening which arises from a lower crystallinity and a smaller particle size.

The particle size distributions of the three LSM powders are given in Fig. 3. The LSM1 powder is composed of a large fraction of sub-micron-sized particles to give a mean diameter of 1.54 μm. A few micron-sized particles are the major constituent in the LSM2 to give a mean diameter of 5.98 μm. The particle size of LSM3 is the largest with a mean diameter of 11.31 μm. The particle size of each LSM can also be visually seen in the electron micrographs shown in Fig. 8(a) to (c).

3.2. Cathodic performances of $La_{0.9}Sr_{0.1}MnO_3$

The cathodic activity of the three LSM electrodes was compared by analyzing their AC impedance spectra which were taken with the LSM/YSZ half-cells at 900°C in air. The spectra obtained with LSM1 are provided in Fig. 4. The spectra are composed of two depressed semi-circles such that the best fitting was achieved with the equivalent circuit depicted in the inset. The circuit is composed of a series combination of a resistance and two parallel combinations of a resistance and a constant phase element (CPE) [14–16]. The equivalent circuit is thus symbolized as $R_1(R_2Q_2)(R_3Q_3)$, where the R and Q represent the resistance and CPE, respectively. The deconvoluted impedance parameters obtained with the data shown in Fig. 4 are listed in Table 1, and the resistance variation with cell operation is separately presented in Fig. 5. The results in Table 1 and Fig. 5 illustrate that R_1 and R_2 are invariant with operation time, while R_3 progressively increases to reach a steady value. From this data, the R_1 component has been assigned to the YSZ electrolyte resistance. The parallel combination of R_2Q_2 that appears as a semi-circle at the higher frequency region is ascribed to the reaction products formed at the LSM/YSZ interface, based on the fact that R_2 increases when the adhesion temperature is further raised. A pyrochlore, $La_2Zr_2O_7$, has been assigned as the reaction product formed at the LSM/YSZ interface in previous reports [17,18]. A support for this assignment is further provided by the n values of Q_2 which are close to unity (> 0.8). As a matter of fact, the CPE of many oxide phases which have no activity for O_2 reduction behaves like an ideal capacitor to give an n value of unity [19]. The R_3Q_3 component which appears as the lower frequency arc is equivalent to a parallel combination of charge-transfer resistance for the cathode reaction and the corresponding CPE. As reported in previous papers [9,20], this component is dependent on the oxygen pressure, which is indicative of being related to the oxygen reduction

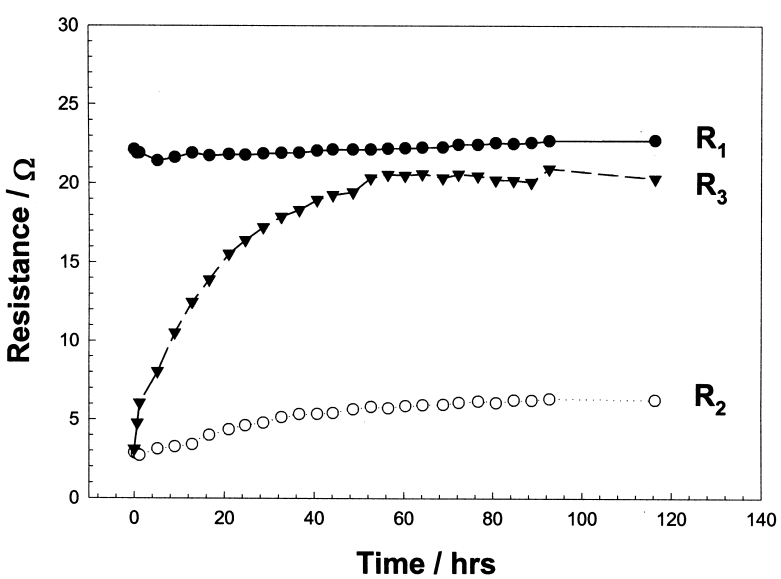

Fig. 5. Evolution of resistances in LSM1 electrode as a function of operation time at 900°C in air. Assignment of the three resistance components is provided in the text.

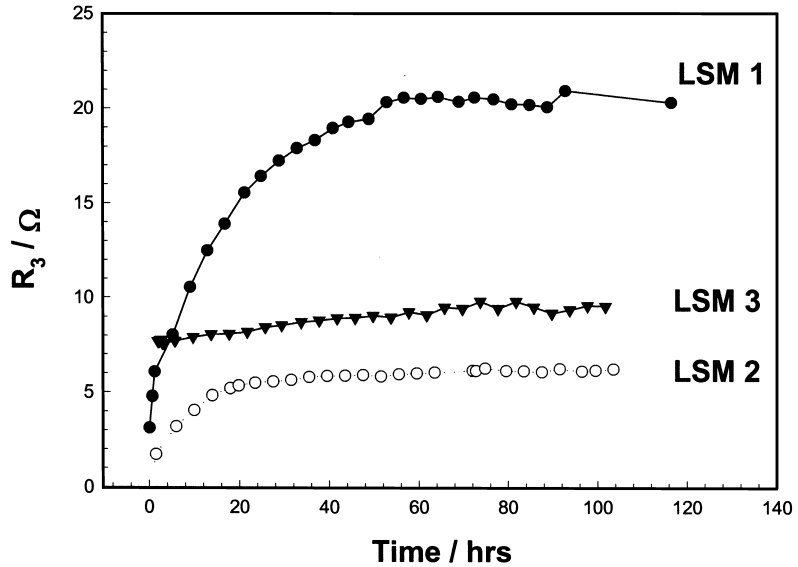

Fig. 6. Variation of charge-transfer resistance (R_3) as function of operation time at 900°C in air for three electrodes.

reaction. The lower n values (< 0.8) of Q_3 are another indication of its relevance to the cathode reaction as the CPE associated with the electrode reaction behaves like a non-ideal capacitor due to the inhomogeneity of the electrode surface [14,21].

The cathodic activity of LSM electrodes was monitored with cell operation by extracting the R_3 values from the impedance spectra (Fig. 6). As seen, the LSM1 electrode displays a low R_3 during the initial period of cell operation, but the value increases rapidly within 60 h. By contrast, the R_3 of the LSM3 electrode is large at the beginning but remains virtually constant, the same even after 100 h of operation. The LSM2 electrode displays the best performance. Its initial activity is better than LSM3, but comparable with LSM1. Although, there appears to be a loss in activity during the earlier stage, the overall activity is better than the others. The relative cathodic activity shown in Fig. 6, viz., LSM1 < LSM3 < LSM2, is confirmed by the steady-state polarization curves which were recorded after 100 h of cell operation (Fig. 7), i.e., the cathodic current increases in the same order.

3.3. Microstructural change in $La_{0.9}Sr_{0.1}MnO_3$ electrodes

Electron micrographs of the electrode surface are shown in Fig. 8. The micrographs in Fig. 8(a) to (c) were taken

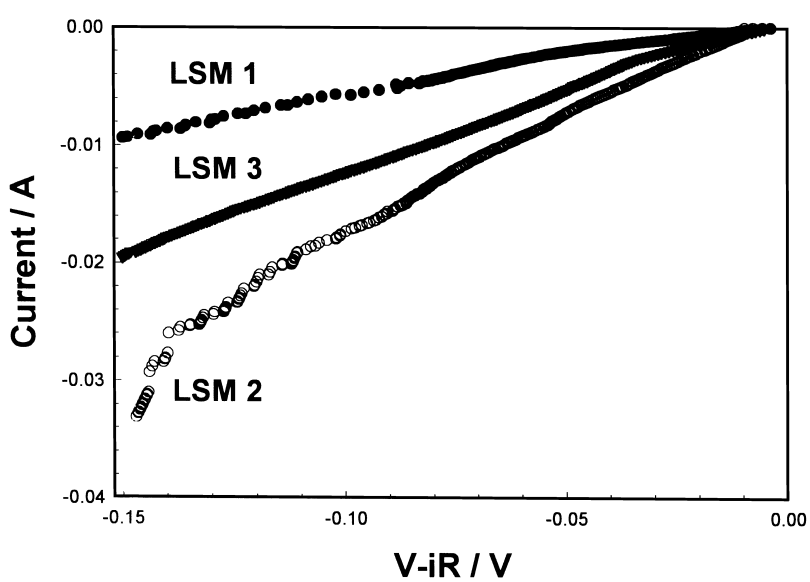

Fig. 7. Steady-state polarization curves for LSM electrodes after cell operation for 100 h at 900°C in air.

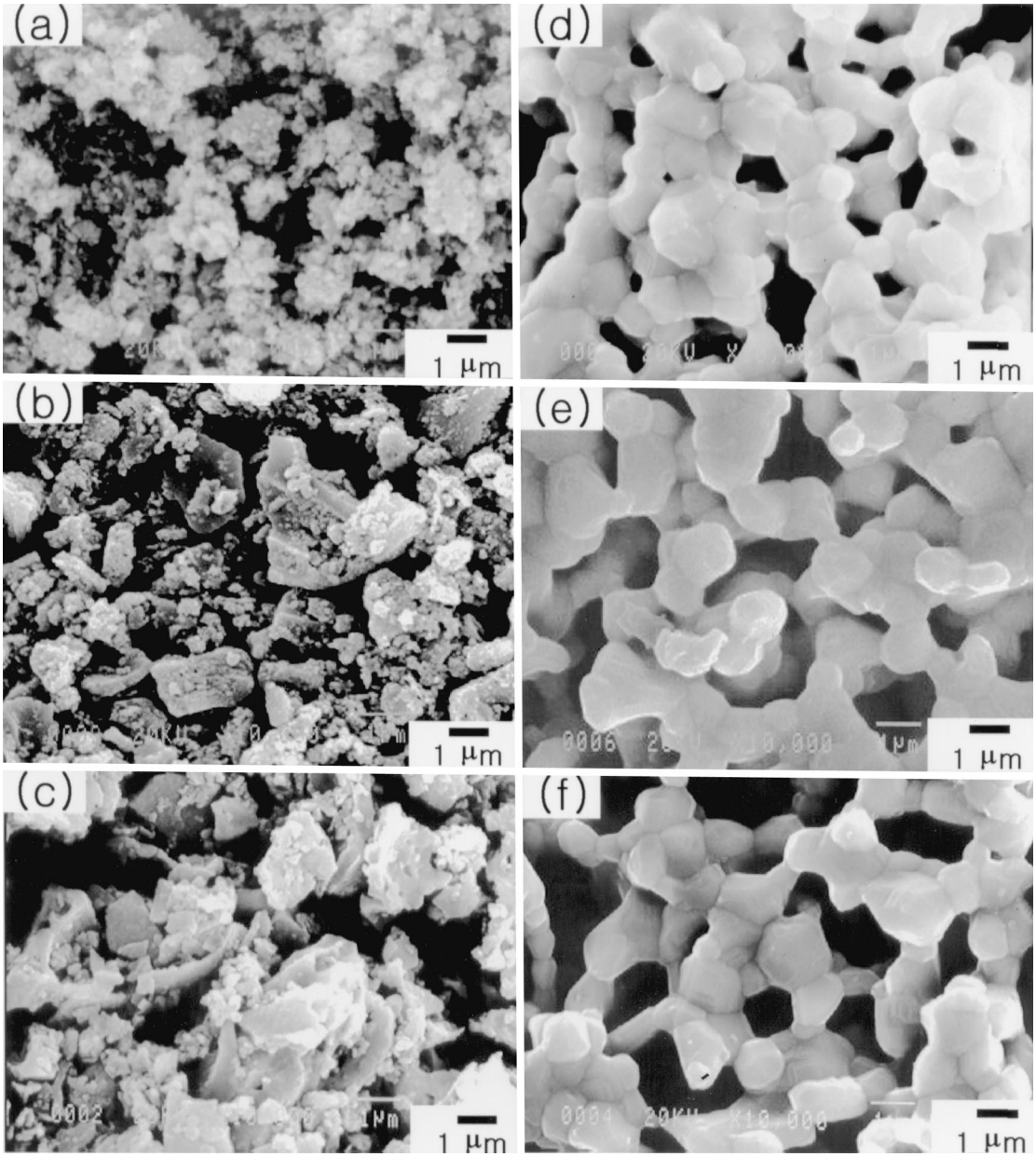

Fig. 8. Scanning electron micrographs of electrode surface: (a) LSM1 after screen-printing; (b) LSM2 after screen-printing; (c) LSM3 after screen-printing; (d) LSM1 after electrode adhesion; (e) LSM2 after adhesion; (f) LSM3 after adhesion.

after the silk printing but before the electrode adhesion step, and thus the starting powders whose size distribution is shown in Fig. 3 can still be observed. As seen, the LSM1 is composed of particles from sub-micron size to a few micrometers, while the presence of larger particles can readily be discerned in the other electrodes. The right panel in Fig. 8 are electron micrographs taken after the electrode adhesion step (1200°C for 2 h). In general, grain growth is observed in each electrode and the particle surface becomes smoother. In detail, particles of < 1 μm are sintered to give a porous layer in the LSM1 electrode. Similarly, the larger particles in LSM2 and LSM3 coalesce, but to a lesser extent, to become a sintered structure.

The variation in cathodic activity shown in Fig. 6 can be correlated with the evolution of the microstructure. As the particle size of LSM1 is the smallest, the best electrode performance is expected with this electrode. Indeed, this electrode gives a reasonably good cathodic activity in the earlier stages of cell operation. But since the grain growth of LSM1 powder is also most significant, its activity rapidly decreases within a short period. Electron micrographs taken after 100 h of cell operation are given in Fig. 9. In the case of the LSM1 electrode (Fig. 9a), the particle coalescence is severe compared with that before cell operation (Fig. 8d). By contrast, a comparison of the electron micrographs in Figs. 8(f) and 9(c) shows that the LSM3

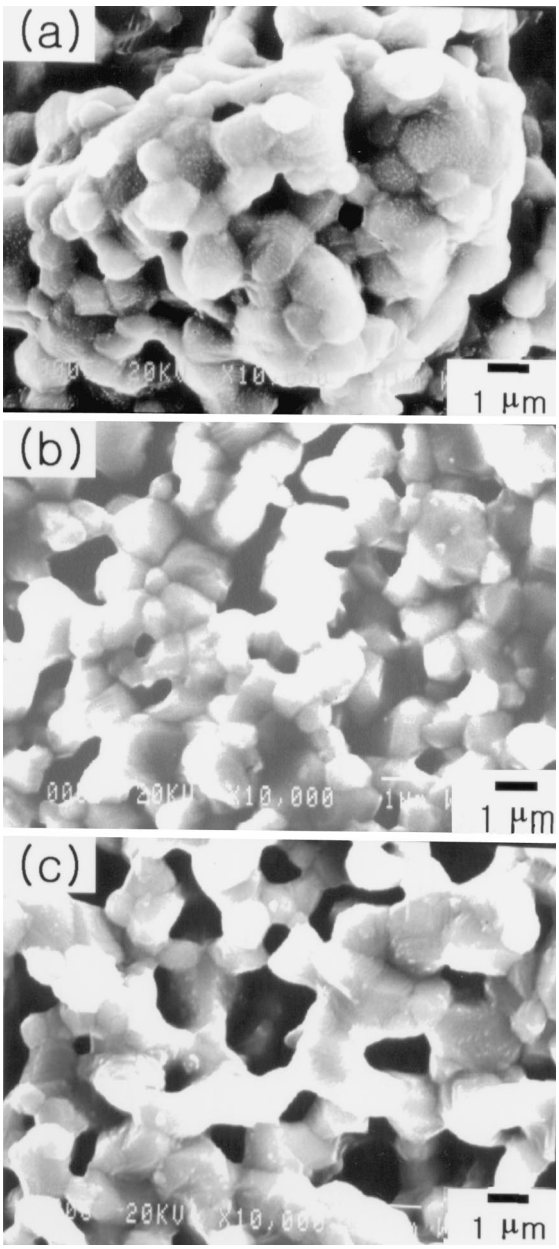

Fig. 9. Scanning electron micrographs after half-cell operation for 100 h: (a) LSM1; (b) LSM2; (c) LSM3. Note severe particle growth in LSM1 electrode.

electrode made with the largest powder experiences insignificant particle growth. Nevertheless, the active sites are not sufficiently plentiful as the particle size is the largest. For LSM2, with a particle size intermediate between LSM1 and LSM3, even if an increase in R_3 is observed during the earlier stages due to particle growth, the overall performance is better than LSM1 because the particle growth is less significant. Also, the activity is better than that of LSM3 because the active sites are more abundant than in LSM3.

4. Conclusions

In this work, three $La_{0.9}Sr_{0.1}MnO_3$/YSZ electrodes have been prepared via silk-printing technique from LSM powders with a mean particle size of 1.54 μm (LSM1), 5.98 μm (LSM2) and 11.31 μm (LSM3), respectively. The LSM powders have a rhombohedral lattice.

The cathodic activity is compared in terms of charge-transfer resistance values. The LSM1 electrode shows a reasonably good activity in the initial stage, but its activity rapidly declines. The good initial activity is attributed to a high population of active sites for the O_2 reduction reaction, either the three-phase boundary or electrode surface sites. The rapid degradation is due to ready sintering of the smallest powder. An electron micrograph taken after 100 h of operation showed severe agglomeration of the particles. The LSM3 electrode gives the worst initial activity due to insufficient active sites but its activity remains largely unaltered due to a negligible change in the microstructure. The LSM2 electrode which was made with the medium-sized powder suffers a slight degradation during the earlier period of cell operation, but its overall activity is the best among the three as the active sites are sufficiently large and particle growth is not significant. A trade-off between the number of active sites and the particle growth rate is likely made at this intermediate size under the present electrode fabrication and cell operation conditions.

Acknowledgements

Korea Science and Engineering Foundation (966-0304-005-2) supported this work.

References

[1] N.Q. Minh, T. Takahashi, Science and Technology of Ceramic Fuel Cells, Elsevier, Amsterdam, 1995, p. 117.
[2] S. Carter, A. Selcuk, R.J. Chater, J. Kajda, A. Kilkner, B.C.H. Steele, Solid State Ionics 53–56 (1992) 597.
[3] K.Q. Huang, M. Feng, J.B. Goodenough, C. Milliken, J. Electrochem. Soc. 144 (1997) 3650.
[4] Y. Takeda, R. Kanno, M. Noda, Y. Tomida, O. Yamamoto, J. Electrochem. Soc. 134 (1987) 2656.
[5] J. Mizusaki, H. Tagawa, K. Tsuneyoshi, A. Sawata, J. Electrochem. Soc. 138 (1991) 1867.
[6] L.G.J. de Haart, R.A. Kuipers, K.J. de Vries, A.J. Burggraaf, J. Electrochem. Soc. 138 (1991) 1970.
[7] A. Hammouche, E. Siebert, A. Hammou, Mater. Res. Bull. 24 (1989) 367.
[8] A. Hammouche, E. Siebert, A. Hammou, M. Kleitz, A. Caneiro, J. Electrochem. Soc. 138 (1991) 1212.
[9] H.Y. Lee, W.S. Cho, S.M. Oh, H.-D. Wiemhöfer, W. Göpel, J. Electrochem. Soc. 142 (1995) 2659.
[10] N.M. Sammes, M.B. Phillipps, J. Mater. Sci. Lett. 12 (1993) 829.
[11] B.A. Boukamp, Solid State Ionics 20 (1986) 31.

[12] S.T. Aruna, M. Muthuraman, K.C. Patil, J. Mater. Chem. 7 (1997) 2499.
[13] V.A. Cherepanov, L.Yu. Barkhatova, V.I. Voronin, J. Solid State Chem. 134 (1997) 38.
[14] J.R. Macdonald, W.B. Johnson, in: J.R. Macdonald (Ed.), Impedance Spectroscopy Emphasizing Solid Materials and Systems, Wiley, New York, 1987, pp. 12–26.
[15] B.A. van Hassel, B.A. Boukamp, A.J. Burggraaf, Solid State Ionics 48 (1991) 155.
[16] F.H. Heuveln, H.J.M. Bouwmeester, J. Electrochem. Soc. 144 (1997) 134.
[17] H. Yokogawa, N. Sakai, T. Kawada, M. Dokiya, Solid State Ionics 40–41 (1990) 398.
[18] H.Y. Lee, S.M. Oh, Solid State Ionics 90 (1996) 133.
[19] S.H. Chu, M.A. Seitz, J. Solid State Chem. 23 (1995) 107.
[20] H.Y. Lee, W.S. Cho, S.M. Oh, Bull. Korean Chem. Soc. 19 (1998) 661.
[21] J.F. McCahn, S.P.S. Badwal, J. Electrochem. Soc. 129 (1982) 551.